AGU PUBLICATIONS

Journal of Advances in Modeling Earth Systems

RESEARCH ARTICLE
10.1002/2017MS001155

A Mathematical Model of Melt Lake Development on an Ice Shelf

S. C. Buzzard[1], D. L. Feltham[1], and D. Flocco[1]

[1]Centre for Polar Observation and Modelling, Department of Meteorology, University of Reading, Reading, UK

Key Points:
- A model has been developed that accounts for the whole lifecycle of surface melt lakes on an ice shelf
- Densification of firn through refreezing meltwater was found to be important for lake formation
- The addition of water from the lake's catchment area and therefore topography were important in lake formation

Correspondence to:
S. C. Buzzard,
s.buzzard@ucl.ac.uk

Citation:
Buzzard, S. C., Feltham, D. L., & Flocco, D. (2018). A mathematical model of melt lake development on an ice shelf. *Journal of Advances in Modeling Earth Systems*, *10*, 262–283. https://doi.org/10.1002/2017MS001155

Received 25 AUG 2017
Accepted 9 JAN 2018
Accepted article online 18 JAN 2018
Published online 3 FEB 2018

Abstract The accumulation of surface meltwater on ice shelves can lead to the formation of melt lakes. Melt lakes have been implicated in ice shelf collapse; Antarctica's Larsen B Ice Shelf was observed to have a large amount of surface melt lakes present preceding its collapse in 2002. Such collapse can affect ocean circulation and temperature, cause habitat loss and contribute to sea level rise through the acceleration of tributary glaciers. We present a mathematical model of a surface melt lake on an idealized ice shelf. The model incorporates a calculation of the ice shelf surface energy balance, heat transfer through the firn, the production and percolation of meltwater into the firn, the formation of ice lenses, and the development and refreezing of surface melt lakes. The model is applied to the Larsen C Ice Shelf, where melt lakes have been observed. This region has warmed several times the global average over the last century and the Larsen C firn layer could become saturated with meltwater by the end of the century. When forced with weather station data, our model produces surface melting, meltwater accumulation, and melt lake development consistent with observations. We examine the sensitivity of lake formation to uncertain parameters and provide evidence of the importance of processes such as lateral meltwater transport. We conclude that melt lakes impact surface melt and firn density and warrant inclusion in dynamic-thermodynamic models of ice shelf evolution within climate models, of which our model could form the basis for the thermodynamic component.

Plain Language Summary Antarctica's Larsen B Ice Shelf, which collapsed spectacularly in 2002, was observed to have a large amount of lakes present on its surface. These lakes were formed through the accumulation of water from melting on the surface of the ice shelf and they have been implicated in the ice shelf's sudden collapse. Such collapse can affect ocean circulation and temperature, cause habitat loss and contribute to sea level rise through the acceleration of glaciers that previously fed onto the ice shelf. We have created a model of the formation and development of these lakes. Using this model, we carry out simulations of the formation of surface lakes on the Larsen C Ice Shelf, located on the Antarctic Peninsula, where melt lakes have been observed. This region has warmed several times the global average over the last century. Our model produces surface melt lakes consistent with current observations. We carry out simulations to determine which processes are most important for melt lake development and provide evidence of the importance of processes such as meltwater transport across the ice shelf to surface lake formation.

1. Introduction

Surface melt lakes have been observed on Antarctic ice shelves, the Antarctic ice sheet (Kingslake et al., 2017; Langley et al., 2016), and the Greenland ice sheet. The presence of these lakes is significant due to their reduced albedo in comparison to the surrounding ice, meaning that they absorb more shortwave radiation and establish an albedo feedback loop that can lead to further melting. A modeling study by Lüthje et al. (2006) found that surface ablation beneath lakes on Greenland was enhanced in comparison to bare ice by between 110 and 170% for the years modeled, values similar to those observed in the field studies of Tedesco et al. (2012), although basal melting from lakes may only contribute a small percentage of overall surface melt and their impact may be limited by lake drainage (Leeson et al., 2015). Therefore, their impact is significant in areas where they are observed. Furthermore, the accumulation and refreezing of water in lake basins leads to changes in the ice shelf temperature and density profiles (Hubbard et al., 2016).

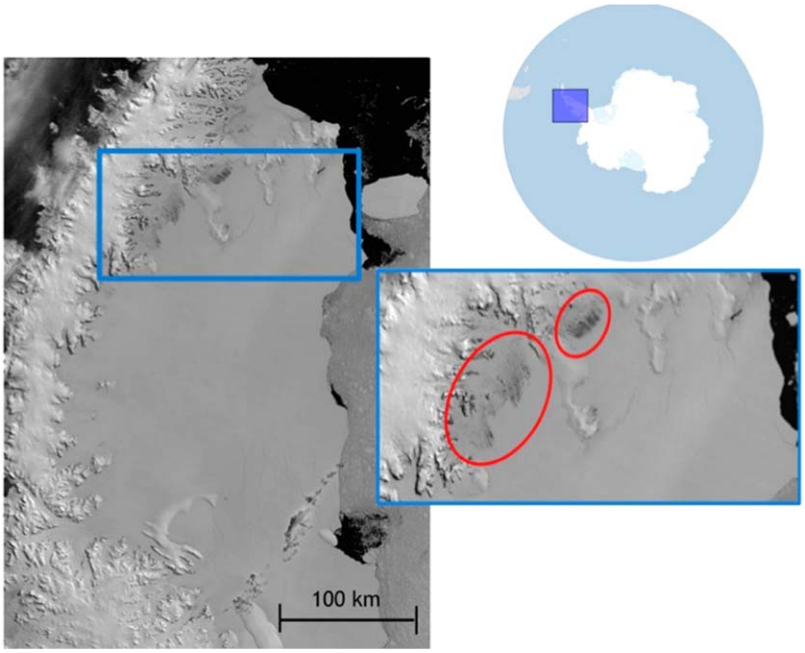

Figure 1. Supraglacial lakes on the Larsen C Ice Shelf in NASA MODIS imagery. The image was captured on 7 January 2007 at 1315. The top right image shows the location of the Larsen C Ice Shelf (created using the Quantarctica software package).

Surface melt lakes have also been implicated in ice shelf breakup. Various mechanisms have been proposed for the role that lakes play in this breakup, including crevasse propagation (Scambos et al., 2003) and ice shelf flexure (Banwell et al., 2013). Figure 1 shows an example of these lakes captured in MODIS imagery on the Larsen C Ice Shelf on the Antarctic Peninsula.

Sudden ice shelf disintegration can lead to losses of vast areas of ice in short periods of time. For example, the dramatic collapse of the Larsen B Ice Shelf in 2002 has been well documented, with 3,200 km^2 of ice being lost during a period of 2 months (Scambos et al., 2004). The loss of the buttressing effect of these ice shelves has been observed to lead to the acceleration of glaciers that previously fed onto the ice shelves, with speed increases of up to 8 times those prior to the collapse (De Angelis & Skvarca, 2003; Rignot et al., 2004), which will lead to an increase in sea level (e.g., the eight glaciers discussed in Rignot et al. (2004) have experienced 27 km^3 [or 24.7 Gt] mass loss per year since 2002). Ice shelf collapse is also important as the addition of the cold, fresh water to the ocean that results from the melting of the collapsed areas of ice can affect ocean circulation, heat budget, and salinity, in addition to causing potential shipping hazards (Gladstone et al., 2001; Silva et al., 2006). Furthermore, ice shelf loss can cause changes in biological habitat (Dimmler et al., 2011).

Modeling melt lakes is important because it can lead to further understanding of the ways that lakes form and how they may develop in the future and alter the surface energy balance of the ice shelf and lead to further melting which can contribute to ice shelf instability (ponds were observed to cover an increasing surface area of the Larsen B Ice Shelf prior to its collapse (Scambos et al., 2000)). Furthermore, it can also lead to their improved representation in ice sheet and climate models to further improve predictions of ice shelf stability and sea level rise.

Previous models of surface melt lakes have often focused on the Greenland ice sheet (Banwell et al., 2012; Leeson et al., 2012; Lüthje et al., 2006) but models have also been developed for ice caps (Clason et al., 2012) and ice shelves (Sergienko & MacAyeal, 2005). Table 1 summarizes the key differences between this work and these existing models. Here we focus on the processes that are important for Antarctic ice shelves such as meltwater retention in firn (this is sometimes ignored in lake models for Greenland where the whole snowfall is assumed to melt and bare ice is exposed before lake formation) and those that will have an effect on the surface energy balance and density of the ice shelf as this allows us to quantify the effect of the lakes on the total melt occurring and investigate their influence on the density profile of the ice shelf.

Table 1
A Comparison of Some of the Features of Existing Melt Lake Models

	Sergienko (2005)	Luthje (2006)	Banwell (2012)	Clason (2012)	Leeson (2012)	Buzzard (2017)
Melting within the lake after formation	✗	✓	✗	✗	✗	✓
Meltwater retention in firn	✓	✗	✗	✗	✗	✓
Effect of lakes on surface energy balance	✗	✓	✗	✗	✗	✓
Lake lifecycle over multiple years	✗	✗	✗	✗	✗	✓
Lateral transport	✗	✓	✓	✓	✓	✗[a]

[a]Although lateral transport is not explicitly modeled, we do include a contribution of meltwater to a lake from a catchment area as described in section 3.4.

Here we present a new one-dimensional model of surface melt and lake development on an ice shelf. This model could in theory be utilized for any ice shelf, here we use the Larsen C Ice Shelf as an example case study where lakes have been observed on the northern part of the ice shelf in MODIS imagery for several years between 2001 and the present day. The model presented aims to improve on previous efforts by including key processes such as melt water retention in firn and modeling the entire lake life cycle over multiple years, which no previous efforts have included. Meltwater retention is important as for lakes to be able to form the firn needs to be impermeable or fully saturated with meltwater. Refreezing will reduce the permeability of the firn for subsequent years, densifying it and reducing the space for meltwater to saturate it, which ultimately can lead to lake formation (Scambos et al., 2003).

This model is the first to explicitly consider the local heat budget in the melt lake and firn and to track phase boundaries as the lake forms, deepens and freezes over. This paper is structured as follows. First, we present the model, describing initially the processes related to surface melt, and then those related to melt lake development and refreezing. We then describe the numerical implementation of the model then present a reference case study of the application on the model to the Larsen C Ice Shelf. This is followed by details of the sensitivity studies carried out on the model. Finally, we present our conclusions.

2. Surface Melt on an Ice Shelf

The model solves the surface energy balance of the ice shelf, calculates heat transfer through the top of the ice shelf and determines the fate of any meltwater that may be produced due to surface melting. The basic model setup is shown in the left-hand diagram of Figure 2. The model is run over a domain of 35 m with 5 cm grid spacing and 1 h temporal resolution.

The surface energy balance and heat transfer are calculated by solving the following system of equations:

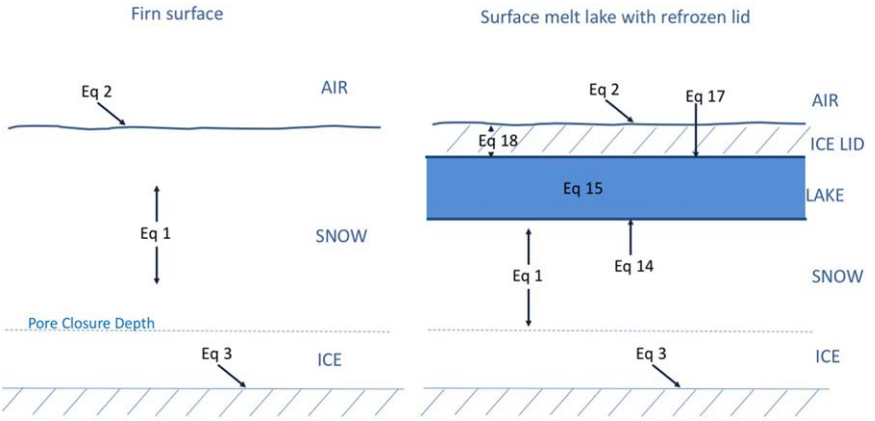

Figure 2. The model setup (left) before lake formation and (right) with a lake and refrozen lid, with references to the relevant equations.

$$\rho c_p^{total} \frac{\partial T}{\partial t} = \frac{\partial}{\partial z}\left(k^{total} \frac{\partial T}{\partial z}\right), \tag{1}$$

for $T(0, t)$:

$$\varepsilon F_{LW} + (1-\alpha)F_{SW} - \varepsilon\sigma T^4 + F_{Sens} + F_{Lat} = \begin{cases} k\frac{\partial T}{\partial z} + \phi\rho_{ice}\mathcal{L}\frac{dH}{dt}, & T = T_{frz}, \\ k\frac{\partial T}{\partial z}, & T < T_{frz}, \end{cases} \tag{2}$$

and for $T(H, t)$:

$$k\rho\frac{\partial T}{\partial z} = 0. \tag{3}$$

Here we have that ρ is density (kg m^{-3}), T is temperature (K; with T_{frz} being the freezing temperature of water), t is time (s), and z is height (m). The specific heat capacity (c_p, J kg^{-1}K^{-1}) and thermal conductivity (k, W m^{-1} K^{-1}) are calculated as a combination of the respective properties for ice and air, depending on the solid fraction of each grid cell, such that

$$c_p^{total} = \phi c_p^{ice} + (1-\phi)c_p^{air}, \tag{4}$$

and similarly for k. Here ϕ is the solid fraction of the firn with density ρ:

$$\phi = \frac{\rho}{\rho_{ice}}. \tag{5}$$

k_{ice} and c_p^{ice} are calculated using temperature dependent formula following Alexiades and Solomon (1993). The air values for c_p and k are calculated following Ambaum (2010) and Moaveni (2010), respectively.

The assumption that there is no temperature change (equation (3)) at the bottom of the model domain is made based on calculations that suggest that temperature changes at the bottom of the ice shelf would not affect the surface of the ice shelf over the time scales considered.

For the surface energy balance, shown in equation (2), α is the surface albedo (taken as the average annual value for the location), F_{LW} and F_{SW} are the incoming longwave and shortwave energy (W m^{-2}), ε is the surface emissivity, and σ is the Steffan-Boltzmann constant (5.67×10^{-8}W m^{-2} K^{-4}). F_{Sens} and F_{Lat} represent the sensible and latent heat fluxes, respectively, and are calculated using bulk formulae, following Ebert and Curry (1993) so that

$$F_{sens} = \rho_a c_{p_{air}} C_T v(T_a - T_0), \tag{6}$$

$$F_{lat} = \rho_a \mathcal{L} * C_T v(q_a - q_0). \tag{7}$$

Here ρ_a is the density of dry air (1.275 kg m^{-3}), c_p^{air} is the specific heat capacity of dry air, T_a and T_0 are the air and surface temperature, respectively, v is the wind speed, q_a and q_0 are the air and surface specific humidities, and $\mathcal{L}*$ is the latent heat of vaporisation, equal to 2.501×10^6 J kg^{-1}. C_T is a function of atmospheric stability following Ebert and Curry (1993) where

$$C_T = C_{T_0}\left(1 - \frac{2b'Ri}{1 + c|Ri|^{1/2}}\right) Ri < 0, \tag{8}$$

$$C_T = C_{T_0}(1 + b'Ri)^{-2} Ri \geq 0, \tag{9}$$

where $C_{T_0} = 1.3\times10^{-3}$, $b' = 20$, and $c = 50.986$ are constants and Ri is the bulk Richardson number, equal to

$$Ri = \frac{g(T_a - T_0)\Delta z}{T_a v_a^2}, \tag{10}$$

where Δz is equal to 10 m.

The rightmost term in equation (2) depends on if the temperature at the surface reaches the melting point. Here $\mathcal{L} = 3.34 \times 10^5$ J kg^{-1} is the latent heat of fusion due to phase change at the surface and $\frac{dH}{dt}$ is the

height change of the surface of the snow due to melting and subsequent percolation of the melt into the snow. Therefore, the term $\phi\rho_{ice}\mathcal{L}\frac{dH}{dt}$ is only activated when melting occurs. The value for the albedo is changed to a wet snow value of 0.6 once melting has begun (Singh, 2001).

The assumption is made that all solar energy is absorbed at the surface. This assumption is also made by Lüthje et al. (2006) for a bare ice surface, and as snow will be highly scattering to incoming shortwave energy that assumption is more valid here.

2.1. Dry Firn Densification

The densification of the firn in the upper layer of an ice shelf is an important consideration due to the dependence of the thermal conductivity, specific heat capacity, and permeability of the firn on density. Furthermore, the pore space available in the snow will need to be known in order to determine at what point the snow becomes saturated with meltwater. Here we calculate snow densification following Arthern et al. (2010). The critical density, 550 kg m^{-3} is taken to be the depth above which the dominant densification processes are grain settling and the packing of snow grains, whereas below this they are sublimation, diffusion and deformation.

The densification model, in a time-dependent form as used by Ligtenberg et al. (2011), and the form that is implemented here, is as follows:

$$\frac{d\rho}{dt}=C\dot{b}g(\rho_i-\rho)e^{\left(\frac{-E_c}{R\overline{T_s}}+\frac{E_g}{R\overline{T_s}}\right)}, \tag{11}$$

where $E_c = 60$ kJ mol^{-1}, E_g=42.4 kJ mol^{-1}, and C are constants, E_c being the activation energy for self-diffusion of water molecules through the ice lattice and E_g being the activation energy for grain growth. C varies depending on whether ρ is above or below the critical density, with values of 0.03 and 0.07 m s^2 kg^{-1}, respectively. $\dot{b}$ is the average annual accumulation (in kg m^{-2} a^{-1}) which is calculated here from reanalysis data. g is the acceleration due to gravity (m s^{-2}), ρ_i is the density of ice (917 kg m^{-3}), T_s (K) is the surface temperature (with $\overline{T_s}$ being the annual average of T_s), and R is the gas constant (8.314 J mol^{-1} K^{-1}). Once melting occurs, percolation and refreezing of meltwater dominates the changes in density. However, as will be shown in section 6.4, the dry snow processes that lead up to this still have an effect on lake formation.

2.2. Meltwater Percolation Through Firn

When melting occurs on an ice shelf the water produced can percolate through the snowpack down until the depth at which the density of the firn is greater than the pore closure depth (830 kg m^{-3}), which is the depth where any remaining air in the firn gets trapped as bubbles within the ice and the firn is therefore impermeable (Ligtenberg et al., 2011).

Surface melt in the model percolates down through the snowpack and refreezes once it reaches a depth within the firn that has a temperature below freezing, where it will refreeze and raise the temperature of its surroundings, with the maximum temperature they can reach being the freezing temperature. The refreezing of meltwater can lead to the development of an isothermal layer; this raises the temperature of the surrounding firn by releasing latent heat (Tseng et al., 1994). Following Tseng et al. (1994), we assume that local heat conduction is an instantaneous process (and as such can occur within one model time step) and that thermoequilibrium is reached instantly with snow at the freezing temperature when meltwater is added. If the temperature reaches the freezing point the remaining meltwater will continue to percolate down to the next layer, excluding a small amount that is retained due to capillary forcing following a similar method to (Ligtenberg et al., 2011).

2.3. Ice Lens Formation

The refreezing of meltwater within the firn causes an increase in density. Once the density of a grid cell reaches the impermeable density (830 kg m^{-3}) then meltwater can no longer pass through that grid cell and an impermeable ice lens has been formed. Once this situation has occurred all further surface meltwater only percolates as far as that grid cell, thus saturating the firn from the level of the ice lens upward, eventually leading to exposed meltwater should sufficient melting occur for the top of the snowpack to become fully saturated.

As the depth of each grid cell in the model is 5 cm it is assumed that once one grid cell of the model reaches the density to form an ice lens (due to refreezing of melt) that this ice lens will then be strong enough to support further saturation of the snow above it. Should the firn become fully saturated and meltwater be exposed at the surface, the model switches to the lake present state as described in section 3.

2.4. Snow Accumulation

Accumulation is added using ERA-Interim data for the location of the automatic weather station being used to provide the data to force the model. As the accumulation data are only available in 12 h time steps, it is assumed that the amount of snow in any one of these time steps is evenly split between each of the 12 one hour time steps that the model runs over.

Accumulation is added at a density of 350 kg m^{-3}, following Kuipers Munneke et al. (2012a). Although this may be slightly denser than fresh snow, the assumption here is made that initial densification of the snow happens very quickly and will not be significant for the modeling results (this is further tested during the sensitivity studies described in section 6).

This new layer of accumulation is added at the air temperature, following Sergienko (2005).

2.5. Refreezing of Meltwater Stored in the Firn

As it is possible for layers that contain meltwater to drop to a temperature below freezing, the meltwater needs to refreeze when this happens. In order to account for this, at the end of each time step the model checks the temperature and water content of each layer. For those layers that are found to contain water and have a temperature below freezing the amount of water needed to refreeze to raise the temperature of that layer to the freezing temperature is calculated. If this is greater than the amount of water present all of the liquid water will refreeze. The density and temperature of that layer are then adjusted to account for this refreezing.

3. Melt Lake Development on an Ice Shelf

Once the permeable snowpack above the pore closure depth (or ice lens) is fully saturated further melting will lead to the formation of a lake. If the temperature at the surface goes over 273.15 K then the surface energy balance is calculated as in equation (2), except that here although the term $\frac{dH}{dt}$ still represents the amount of ice that melts, the height of the surface does not reduce as the melted ice just stays in place as it can no longer percolate vertically and only the density of the layer changes. Since the term ϕ takes into account the fraction of each layer that is solid, the speed at which the surface layer melts depends on how much solid ice there is in it.

This melting is assumed to continue in this way until the lake is 10 cm deep, and then the model switches to a lake development phase, as described in section 3.1. The value of 10 cm was chosen as it is high enough for the lake to become convective (see section 3.1) and large enough that it was not found to often refreeze soon after it has formed which was found to be the case during initial testing of a 5 cm threshold, which also guaranteed convection but was found to often refreeze rather than develop into a deeper lake.

3.1. Melt Lake Development

Once the top 10 cm of the saturated firn has fully melted, a lake is taken to be present. The surface temperature of the lake is determined as the solution of

$$F_{LW}+(1-\alpha)F_{SW}-\epsilon\sigma T^4+F_{Sens}+F_{Lat}+F_c(T)=0. \tag{12}$$

The value of the albedo for the lake is taken to be equal to

$$\alpha=\frac{9,702+1,000e^{3.6h}}{-539+20,000e^{3.6h}}, \tag{13}$$

where h is the height of the lake, following Lüthje et al. (2006).

The movement of the boundary between the top of the firn and the bottom of the lake is described by a Stefan equation, as follows:

$$\phi\rho\mathcal{L}\frac{\partial h_l}{\partial t}=k\frac{\partial T}{\partial z}+F_c(T_l). \tag{14}$$

Here h_l is the location of the boundary between the lake and the firn and T_l is the temperature at that boundary.

Following Taylor and Feltham (2004), a Rayleigh number of 630 is taken to be the critical value over which the lake becomes turbulent and, since this is exceeded as soon as a 10 cm lake forms, the lake has a well mixed core of constant temperature. The temperature within the lake is calculated as

$$(\rho c)_l h\frac{\partial \bar{T}}{\partial t}=-F_c(T_l)-F_c(T_u)-\int_{h_l}^{h_u}F_{net}(z)dz, \tag{15}$$

where h is the lake height (m), $(\rho c)_l$ is the volumetric specific heat capacity of water, and $F_{net}dz$ is calculated using Beer's law to account for the attenuation of shortwave radiation as is passes through the lake.

The heat fluxes directed outward at the boundaries of the lake, $F_c(T_l)$ and $F_c(T_u)$, are calculated using the four-thirds law for turbulent convection:

$$F_c(T^*)=\mathrm{sgn}(\bar{T}-T^*)(\rho c)_l J|\bar{T}-T^*|^{4/3}, \tag{16}$$

where T^* is the boundary temperature, $\bar{T}$ is the average temperature in the lake, and J is the turbulent heat flux factor, equal to 1.907×10^{-5} m s^{-1} K$^{-1/3}$.

The temperature profile of the firn continues to be calculated as described above, except that now the surface temperature of the firn is held at 273.15 K due to that being the location of the firn-lake boundary.

3.2. Refreezing of the Lake

When the surface energy balance becomes negative the lake starts to refreeze and an initial lid of ice is formed on top of the lake. This model setup is shown in the right hand side of Figure 2.

It is likely that in reality, the ice lid may form, melt, and reform several times due to temperature oscillations before the lake presents a stable ice cover. It is assumed here that once a lid is present it does not melt, but in order to minimize errors, we have assumed that the model only switches from a melting to freezing state when a "virtual" lid of at least 10 cm forms. This happens when enough consecutive time steps with freezing conditions occur. The amount of freezing that would take place in each time step is calculated and the total is recorded. Only when this total reaches 10 cm does the model switch to a freezing state. The temperature profile of this virtual lid is also recorded so that should it become a permanent lid it will be assigned this temperature profile. This allows the melting and refreezing of lids to be taken into account without having to build a significantly more complicated model as melting on top of the lid could occur, leading to several layers of the model.

The surface temperature of the lid is calculated to satisfy equation (2).

The development of the lid-lake boundary is treated as a Stefan problem:

$$\rho_{ice}\mathcal{L}\frac{\partial h_u}{\partial t}=k\frac{\partial T}{\partial z}+F_c(T_u). \tag{17}$$

The temperature of the lake, firn below the lake, and development of the lake-firn boundary are all calculated as above.

While the lid is smaller than 10 cm its temperature profile is taken to be linear. Once a permanent lid is established, the temperature profile through the lid is determined following the equation below:

$$\rho c_p^{ice}\frac{\partial T}{\partial t}=\frac{\partial}{\partial z}\left(k^{ice}\frac{\partial T}{\partial z}\right)+(1-\alpha)e^{\frac{-\kappa^* z}{\mu}}F_{SW}. \tag{18}$$

The rightmost term in equation (18) represents absorption of shortwave radiation within the ice lid, it is included here as the surface here is bare ice, so will reflect less shortwave radiation than snow which is highly scattering. Here κ^* is the extinction coefficient (or absorptivity), set equal to 1 m^{-1} and μ is the cosine for the effective angle for incident sunlight, taken to be 0.5 following McKay et al. (1994). The value

of α is taken to be 0.431, following the upper end of the measurements taken by Henneman and Stefan (1999) as the lakes considered here are shallower than that measured in their study.

3.3. Extending the Model to Multiple Year Runs

The change in density of the firn due to the formation and refreezing of meltwater may have consequences for the formation of future lakes. In order to account for this the model can be run over multiple years. For the case where a lake does not form this is reasonably straight forward; the model can just continue to run as it is if exposed water does not become present as everything is contained within a single layer of the model. For the case where exposed water is present but a lake does not develop the model switches back to a state of assuming there is no water at the surface (i.e., it has all refrozen) after 24 h of the surface temperature being below freezing. When a lake has formed and fully refreezes the firn and refrozen lid profiles are combined, allowing the model to proceed as initially, but with an area of solid ice within the firn which insulates the firn below it, delaying the refreezing of the remaining meltwater.

3.4. Transport of Water From a Catchment Area Into a Lake

The topography of the ice shelf will determine which areas of the ice shelf meltwater will pool in and thus may be locations for lakes. Luckmann et al. (2015) suggest that one of the reasons for the rapid filling of lakes they observed is flow of water across the ice shelf in periods of intense melt. In order to account for this accumulation of melt water in certain areas, the amount of available meltwater in a catchment area around the lake is calculated. A separate firn column is modeled for the catchment area, where the model proceeds as described above but any meltwater produced is assumed to percolate out of this column and the volume of this meltwater is used to calculate how much water would be added to the lake from lateral transport. As all the surrounding firn is assumed to melt at the same rate this is equivalent to multiplying the 1-D firn melt rate (with no exposed lake) by a melt multiple.

Here we make the assumption that water will not reach the lake from the catchment area until an ice lens is formed. This is because during the period of meltwater percolation and refreezing in the model domain, refreezing will occur in the surrounding firn too. It is only once an ice lens has formed that water will be able to flow through the isothermal catchment area and accumulate in the lake basin. Subsequent to ice lens formation, all additional meltwater produced is removed from the catchment area firn column and added to the lake basin firn column after having been multiplied by the melt multiple, which is determined by the lake catchment area.

The size of the catchment area is calculated by multiplying the speed of fluid flow, given by Darcy's law for fluid flow through a porous medium, by the total time that melt occurs after lens formation, which can be determined by initial model runs. For the reference case study presented below we assume a surface gradient on the ice shelf of 0.05 (based on a the range of values found within a Digital Elevation Model provided by Susan Bevan, University of Swansea), which gives a speed of 9×10^{-4} m s^{-1} and a distance of 735 m that meltwater can travel during the given melt period. From this, a total catchment area can be determined and the factor with which melt should be multiplied by when added to the lake basin can be calculated by comparing the lake surface area with this catchment area. Here we take an example lake size from Landsat imagery, and find a melt multiplier value of 6 for the reference case study.

This approach assumes a closed basin and is therefore a key area for future model development as it would not hold in all locations. For example, lakes such as those described in Kingslake et al. (2017) and Bell et al. (2007) form part of an active hydrological network. This means that water may flow faster in some areas (e.g., through channels) and the assumption made here of uniform meltwater flow through the catchment area would not hold. Furthermore, the catchment area may change as ice flows so in a faster flowing area or over longer time periods this may become significant.

4. Numerical Implementation of the Model

The surface melt model has been created using Matlab, with all results stated here calculated using Matlab version 2015a. It consists of a main module from which the code can be run, which calls several functions depending on the status of the model.

To solve equation (1), Matlab's inbuilt partial differential equation solver *pdepe* is used. This solver uses the method of lines, a finite difference method (MathWorks, 2015; Skeel & Berzins, 1990). The algorithm to determine the fate of percolating meltwater is run in between time steps of the solution of the above system. In order to take into account height changes due both to melting and accumulation, a front fixing coordinate transform is used following Crank (1984).

The model is initially run over a 35 m profile which is allowed to change to account for surface melting and snowfall. This depth was chosen as during initial testing this was the minimum size of domain where temperature and density changes were not found to reach the bottom of the model domain. The model resolution of 5 cm grid spacing was chosen as it was found that results for resolutions of 5 cm and below were identical and therefore 5 cm was chosen as the resolution for the model in order to minimize the time taken for the model to run (Buzzard, 2017a). The vertical domain is allowed to change to account for surface melting and snowfall.

The lake and any subsequent frozen lid of ice that forms on top of the lake are taken to have 20 grid cells each, spread equally over the height of the lake or lid. The actual size of these grid cells is therefore constantly changing with the growing and shrinking of the lake and lid.

The code was initially tested using prescribed forcing and the model was found to conserve mass with an accuracy of 99.7% and conserve energy during the solution of the heat equation with an accuracy greater than 99.9% (Buzzard, 2017a).

5. Reference Case Study

Surface melt lakes have been observed on the Larsen C Ice Shelf, the southern neighbor of the Larsen B Ice Shelf. Alongside other Peninsula ice shelves it too has been experiencing warming, resulting in the −9°C isotherm, which has been suggested as being the northern limit of ice shelf viability (Morris & Vaughan, 2003), having now moved far enough south to cross the Larsen C Ice Shelf. It has been suggested to be one of the most susceptible ice shelves for sudden collapse based on melt activity (Scambos et al., 2000), firn characteristics and melt season length (Scambos et al., 2004), and the incidence of lake occurrence may increase under a warming climate.

In order to simulate lake formation on the Larsen C Ice Shelf, the model described above was forced using automatic weather station (AWS) data provided by the British Antarctic Survey (BAS) for the time period May 2010 to April 2011 at latitude −67 longitude −61.47. The only information not available that is needed for the model was humidity. For this, values were taken from Kuipers Munneke et al. (2012a), where the average value for each season is used.

The location of the AWS data available is further downstream on the ice shelf than the lakes that are visible in the MODIS imagery. One key issue with this is that the areas where the lakes are present are close to the Peninsula mountains and are particularly affected by foehn winds. These are warm, dry downslope winds that bring warm air down to near to the surface of the ice shelf, flushing away cool air that may be present. Foehn winds have been found to be associated with exceptionally high melt rates on the Larsen C Ice Shelf (Kuipers Munneke et al., 2012a) and therefore are an important process that needs to be considered when modeling surface melt on the ice shelf.

Running the model using only the AWS information available did not lead to lake formation. The firn surface does reach the melting temperature and some densification of the upper part of the firn does occur, but this is far from an amount sufficient for ice lensing or saturation of the firn. This suggests that the model is replicating the conditions on the ice shelf where the forcing originated from and where lakes have not been observed, and means that further processes need to be included in order to be able to use the model to study lake development on the Larsen C Ice Shelf with the data available.

In order to replicate the conditions found closer to the grounding line of the ice shelf where the lakes are found, a foehn wind effect was added in to the atmospheric forcing data. Following the modeled values found in Luckmann et al. (2015), it was estimated that the areas where lakes were formed had an average temperature of up to 7 K higher than the AWS location during foehn wind events, and an average wind speed of up 10 m s^{-1} greater that the AWS location. For the 2010–2011 melt season, foehn conditions were

seen for around 30% of the time between January and March 2011 (Luckmann et al., 2015). However, foehn events that were measured directly on the Larsen C Ice Shelf were found to be cooler and with a lower wind speed (J. Turton, personal communication, 2013). Therefore, based on this information, a foehn effect is added into the model by increasing the air temperature by 5 K and the wind speed by 5 m s^{-1} for 18 h in each 52 h period between the months of January and March. The importance of these values is tested during the sensitivity studies in section 6.

In order to investigate the effect of multiple years of melt, the model is set up to loop over the 2010–2011 data so that the model experiences multiple melt seasons with the same forcing conditions.

5.1. Initial Conditions

The initial density profile used in the firn is that given following Paterson (2000), using the formula of Schytt (1958):

$$\rho(z)=\rho_{ice}-(\rho_{ice}-\rho_{sfc})e^{-cz}, \tag{19}$$

where ρ_{sfc} is the density at the surface and $c=1.9z_t$, with z_t being the location of the firn-ice transition. For the Larsen C Ice Shelf, the measured value of 37 m from Jarvis and King (1995) was used.

The suggestion that the firn-ice transition (which is equivalent to the pore closure depth) is at 37 m below the surface does mean that full saturation of the firn in the model is not possible using a vertical profile of only the top 35 m, which was the model domain chosen here. However, during initial testing, it was confirmed that an ice lens consistently forms at depths higher than 35 m using this density profile and a range of surface conditions, so full saturation of the firn down to the pore closure depth would not happen in this situation. It is suggested that if the model is used for a different location, then the model domain would need to be extended to below the pore closure depth for that area at least for initial testing.

An initial surface density of 500 kg m^{-3} was used as this was observed on the ice shelf during the period where much of the weather station data used here were available (B. Kulessa, personal communication, 2013).

The initial temperature profile is linear, starting at 253 K at the surface and increasing to 263 K at the bottom of the model domain. These values were chosen based on firn core data from a field expedition to Larsen C in 2009–2010. Here the temperature was found to reach 264 K between 25 and 30 m in the snow, with a minimum temperature recorded of 263.5 K. Unfortunately there were no firn cores taken deeper than 30 m so a bottom value here of 263 K was chosen as temperature did not change very much below the top 20 m in either profile. Although the firn cores were taken during the summer and the model is run starting in the Antarctic winter it is expected that these values from deeper in the ice shelf will not vary a great deal seasonally through heat conduction. However, this does mean that the firn cores cannot provide useful information about the winter surface temperature and therefore it is taken to be close to the value for the MAM average given in Kuipers Munneke et al. (2012a).

5.2. Results

The model is run with the inclusion of the foehn wind effect and lateral melting. Inclusion of both of these effects was found to lead to consistent lake development in each year after an initial spin-up period. An ice lens was found to form during the first year as demonstrated in Figure 3. This figure also shows the isothermal temperature layer that forms from the surface down to the level of the ice lens which has a density of the pore closure. The isothermal layer remains stable from the time that it forms, other than fluctuations in the top meter, mostly due to diurnal temperature variations. The retention and saturation of water in the firn is shown in Figure 4. Figure 5 shows the retention of water subsequent to saturation, due to the capillary effect.

Subsequent to lens formation, saturation of the firn occurs from the lens upward, meaning that less meltwater is required to fully saturate the firn than if the lens had not been present.

Subsequent to the initial lake forming the refrozen lake acts as an impermeable ice lens for later lakes, reducing the depth of snow that needs saturating and bringing forward the time of lake exposure and also insulating the firn below. The development of these lakes over 10 years is shown in Figure 6. Over the 10 years shown here there was a total of 6.09 m of water equivalent firn melt. If we take the spin-up period to be 5 years we have for the final 5 years an average lake depth of 1.24 m and a maximum lake depth of

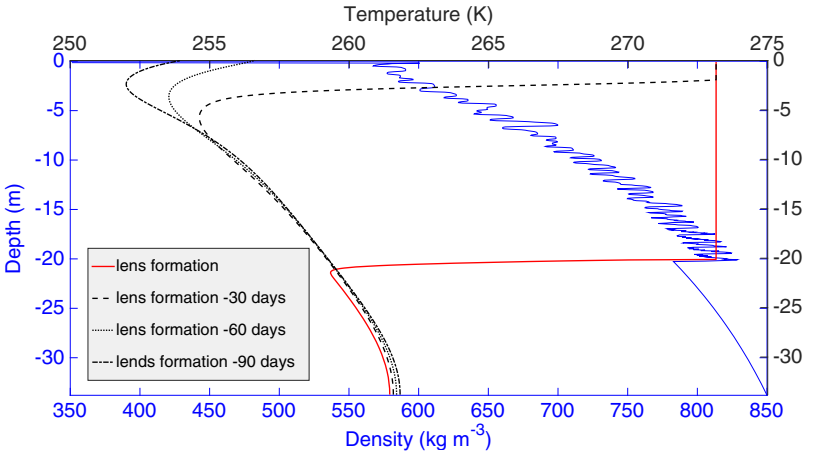

Figure 3. The density profile (blue, solid) and temperature profile (black, solid) at the time of ice lens formation (25 December in the first year of the simulation). Here it can be seen that the depth of the ice lens with a density greater than that of pore closure coincides with the bottom of the isothermal temperature profile. The temperature profiles in the lead up to this (30, 60, and 90 days before lens formation) are shown in black (dashed, dotted, and dash-dotted lines).

1.29 m. It was found that the lake height begins to stabilize after 3 years, with very similar profiles present in subsequent years as the model appears to reach a steady state. This is to be expected as the model is run using the same forcing each year, and once deeper lakes have developed lakes in subsequent years do not melt all the way through the solid ice of the previous year's refrozen lake so the conditions during each year are very similar.

The sharp increases in surface height of the lakes are due to lateral transport of meltwater. The amount with which lateral transport of melt from the catchment area contributes both to firn saturation and to the

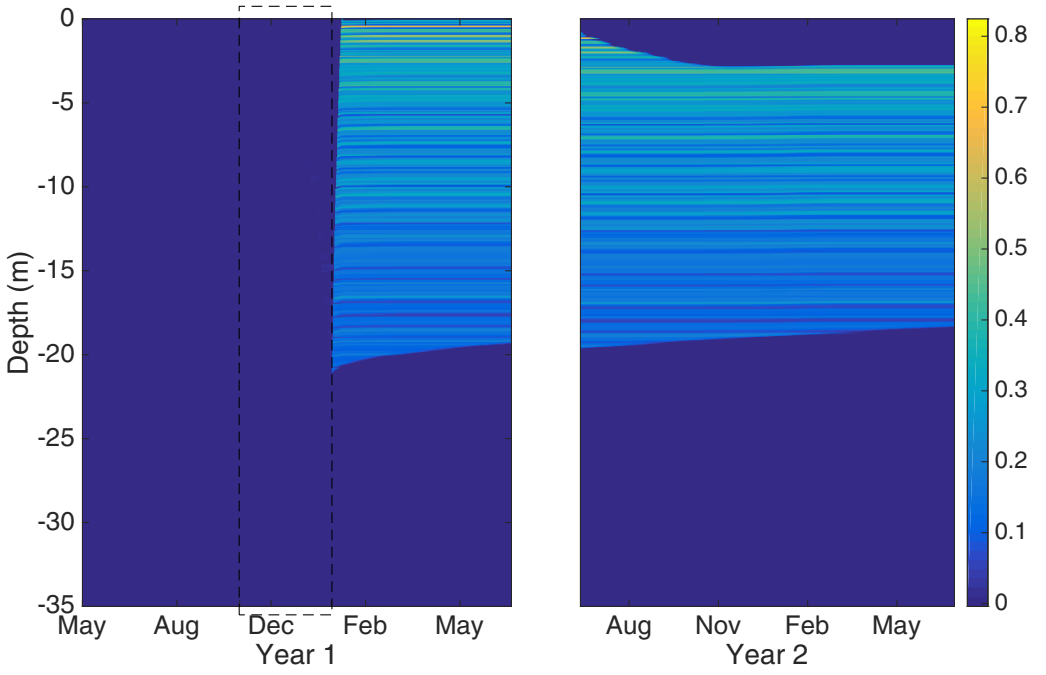

Figure 4. The development of the water content profile of the firn layer over the first 2 years of the model simulation. The split in the figure occurs when the lake from the first year has fully refrozen and this solid ice is added to the firn profile. The color bar shows the water content as a fraction of each grid cell. The black dashed rectangle shows the time period covered by Figure 5.

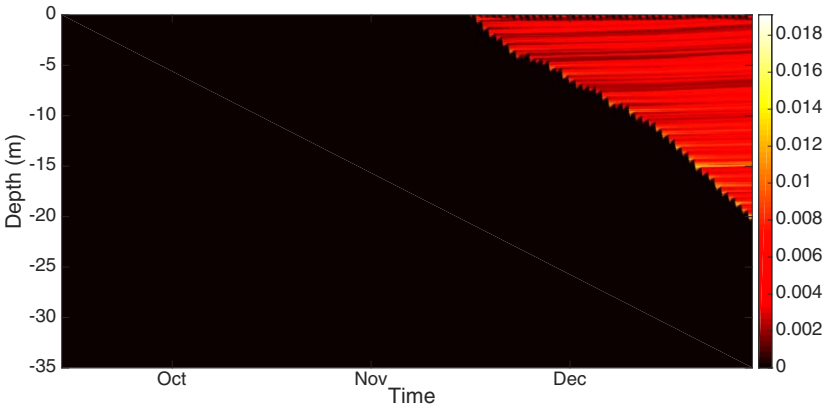

Figure 5. The water content of the firn during the period in the first year of the simulation before ice lens formation where the only liquid water present has been retained due to capillary forcing. The color bar shows the fraction of each grid cell that consists of liquid water.

increase in depth of the lake shown here demonstrates that it is a key process in both lake formation and development.

The surface height initially decreases and firn is melted and saturated with meltwater. However, beyond the spin-up period the surface height increases each year due to the addition of meltwater from the catchment area that refreezes in the lake area. This would be expected from constantly adding meltwater and the repeated use of forcing data from a warm year, so this increase of height would not be expected under present day conditions as warmer years do not always immediately follow each other for an extended period.

Figure 7 shows the density profile of the firn for the first year. The initial small increase in density from the surface down beginning toward the end of November is due to the freezing of meltwater percolating down into the firn and the small fraction of meltwater that is retained due to capillary forcing as the meltwater passes through the upper snow layers.

An ice lens forms at 20.23 m below the surface and subsequent to this there is a small amount of increase in density due to firn densification and refreezing of meltwater which reaches firn that is below the freezing temperature. The density then starts to sharply increase from the lens level upward as the firn above the ice

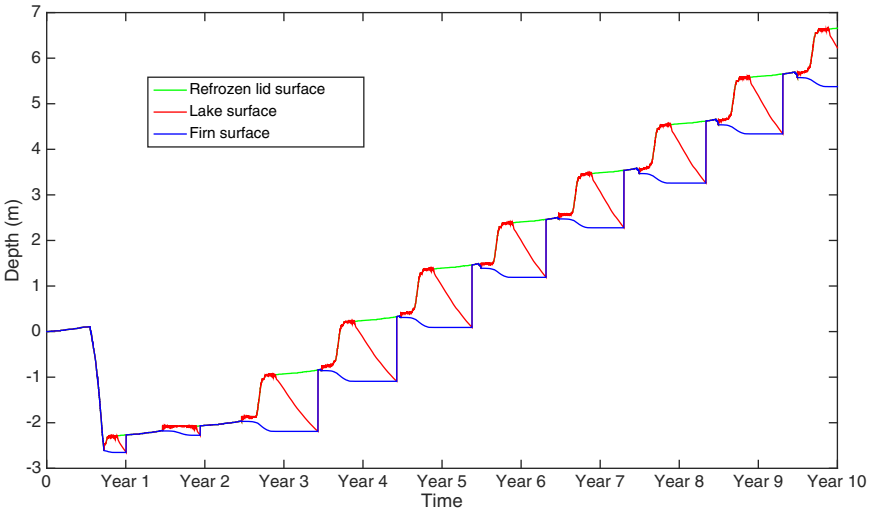

Figure 6. The development of surface melt lakes over a 10 year model run using 2010–2011 data. Here the blue line shows the firn surface, the red line the lake surface, and the green the refrozen lid. On the vertical axis 0 is the initial ice shelf surface and all subsequent hights are shown relative to this, hence the height increase due to snowfall and the additon of water from the catchment area. Basal melting of the firn can be observed once lakes have formed.

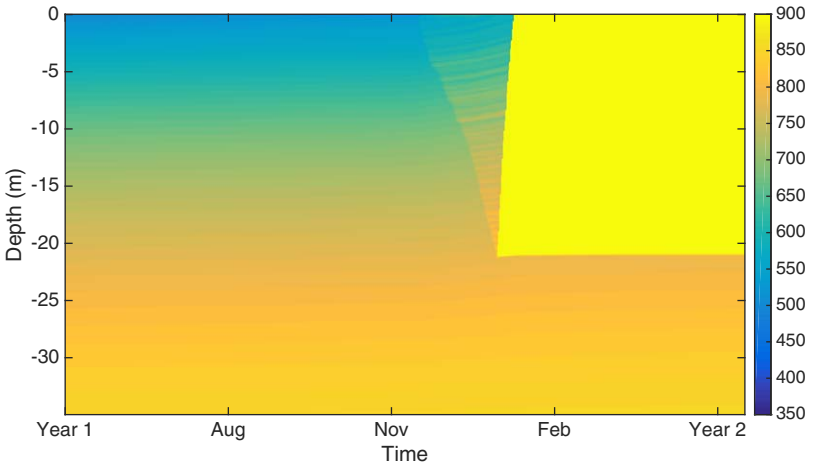

Figure 7. The development of the density profile of the firn over the first year of the model simulation. The color bar shows the density in kg m^{-3}. The vertical label on the left-hand side is the initial depth. In reality, these depth values will change from left to right along the plot with time but due to a coordinate transform used we can directly compare the profiles. However, it was felt that including the initial depth on the left-hand axis was helpful to give a sense of scale.

lens becomes saturated with meltwater. This large block of high density (shown as the yellow area in Figure 7) persists for the remainder of the simulation. Small areas of low density appear at the surface as fresh snow falls, but each year they are melted and incorporated into a new lake, which is able to form more quickly as there is a much smaller depth of snow to melt or saturate.

5.3. Model Validation

Surface melt lakes are visible on the Larsen C Ice Shelf in NASA's MODIS (Moderate Resolution Imaging Spectroradiometer) imagery for multiple years during the period from 2001 to mid-2016. The lakes show clearly as dark features, as can be observed in Figure 1.

The number of melt days that occur in the model simulation presented here matches well with those from Envisat data (Luckmann et al., 2015). Ensuring that these days match the onset times of lake formation could be possible using MODIS imagery but is difficult due to the sparse temporal availability of clear MODIS imagery. For the year examined (the 2010–2011 melt season) there is no clear evidence of lake onset day, although there is a clear image of lakes in mid-November. The lake onset days given by the model are toward the beginning of November each year and this corresponds well with the evidence available for lakes from 2005 to 2009 where lakes often form in November or December.

Ice lenses have been observed in the firn on the Larsen C Ice Shelf (Hubbard et al., 2016). It was found that ice lenses were present in the firn in Cabinet Inlet during the 2014–2015 field season in a distribution that appears to resemble annual layering. This suggests that even if lakes were not forming in the years immediately previous to this, melting and refreezing within the firn was still occurring and these processes may therefore be important in firn densification and lake formation in subsequent years. Similar annual layering was observed during a separate field expedition on Larsen C by Gourmelen et al. (2009).

NASA's Landsat program has acquired data that can be used to look at both the distribution and the depth of lakes on the Larsen C Ice Shelf. In order to verify that the availability of lake free areas surrounding lakes matches or exceeds that needed for a catchment area of the size a comparison of the ratio of "lake" pixels to "ice" pixels is calculated from a small area shown in Figure 8 where multiple lake forms are present. This area was chosen due to it being densely populated with lakes and therefore can be taken to be a minimum value of this ratio. Even in this area we have a ratio of approximately 1:40, suggesting that the melt multiplier value of 6 used here is well within the bounds of the available catchment area and that it is the distance water can travel rather than the volume of available water that constrains lateral transport.

In addition, lake depths can be calculated from Landsat 8 imagery (Pope et al., 2016). The data from the scene shown in Figure 8 were used to create Figure 9. The average lake depth from this area was 0.52 m

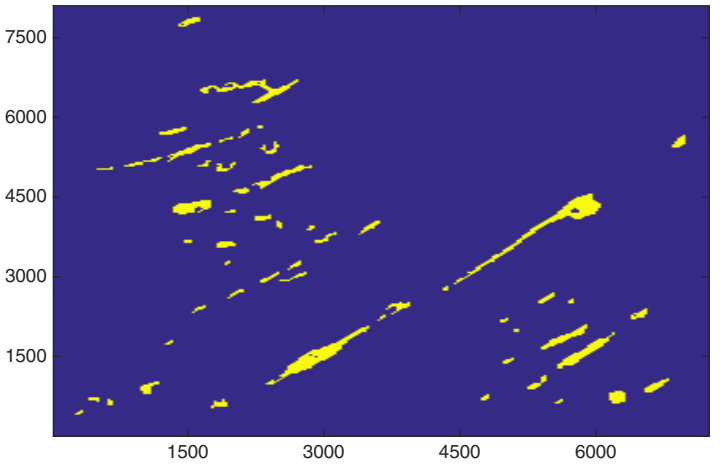

Figure 8. Landsat image of a section of the Larsen C Ice Shelf where melt lakes were present on 6 January 2016. Both axes have units of meters. Here the lakes are colored yellow and areas where lakes were not present are colored blue. Although these data were taken from the Landsat 8 mission so is from a later time than the lakes examined using the 2010–2011 melt season, it is likely that the lakes will be similar in many aspects due to the role of topography in the location of lake basins.

and it can be seen from Figure 9 that the spread of lake depths is concentrated around the 0.1–1.3 m range, suggesting that the lake depths found by the model are, given the level of accuracy of this method (estimated by Pope et al., 2016 to be 0.0 ± 1.6 m), within realistic bounds. Given that the modeled lakes are created by repeatedly forcing the model with data from an unusually warm melt season it is unsurprising that their maximum depths are toward the deeper end of these values.

For the time period of data available used to force the model, the Landsat 7 satellite would have been in use rather than Landsat 8 which was used for the Pope et al. (2016) study and for the data shown in Figures 8 and 9. However, further work has been done to use this method for Landsat 7 data which gave average lake depths ranging from 0.34 to 0.47 m for various scenes analyzed for the period 2007–2009 and similar ranges of values to those from Figure 9. Although this method is less tested than the use of this technique for Landsat 8 data, it is nevertheless useful to see here that the lake depths calculated during this modeling study again match reasonably well with the ranges and averages calculated from the Landsat data even if processed images were not available for the exact time period modeled.

6. Sensitivity Studies

In order to determine the sensitivity of modeling results to various uncertain parameters, the model was run many times changing one parameter each time, and these runs compared with the reference simulation described in section 5.2. Ten years was deemed an appropriate length of time to carry out sensitivity simulations as it was found that the lake volume quickly becomes quite consistent in the reference simulation (see Figure 6), and 10 years allows for a 5 year spin-up period plus 5 years of simulations to compare after this spin-up period. The results of these studies are summarized in Table 2.

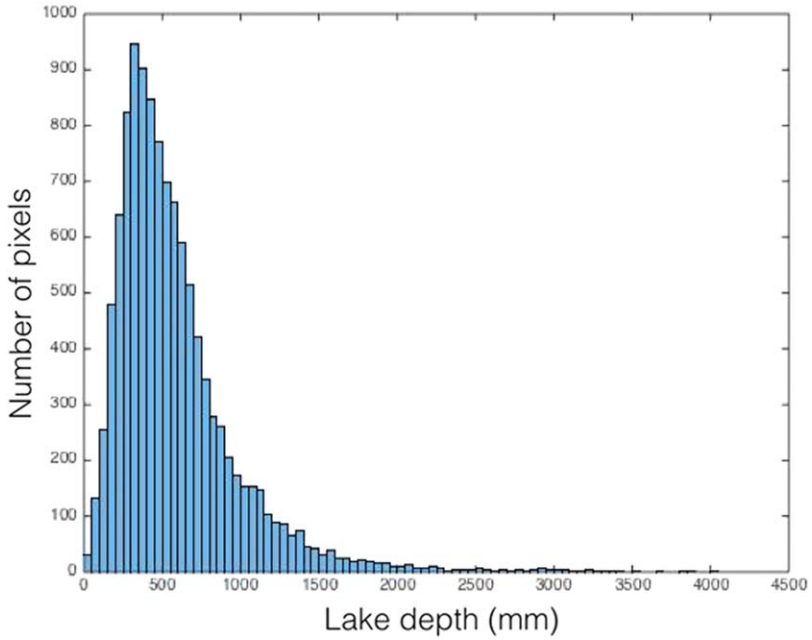

Figure 9. Lake depths on the Larsen C Ice Shelf as calculated from Landsat data from 6 January 2016. The horizontal axis gives lake depths in mm and the vertical axis gives the numbers of pixels for each depth. This figure has been reproduced with permission from calculations carried out by Allen Pope (NSIDC).

Table 2
The Reference Case Parameter Values or Ranges, Sensitivity Study Parameter Values, and Results From the Sensitivity Studies

Parameter	Reference case value/range	Sensitivity study	Average lake depth (m)	Maximum lake depth (m)
Reference case			1.24	1.28
Air temperature (K)	228.6–287.0	+0.5 K	1.08	1.11
		−0.5 K	1.34	1.39
Melt multiple	6	3	0.67	0.78
		9	1.68	1.77
Accumulation (m)	0.4952	×0.5	1.11	1.33
		×2	1.30	1.35
Snow density (kg m^{-3})	350	300	1.24	1.29
		400	1.11	1.14
Dry snow densification	n/a	0	1.27	1.32
Foehn wind speed (m s^{-1})	5	0	1.19	1.30
		10	1.19	1.25
Foehn wind temperature (K)	5	3	1.19	1.24
		7	1.37	1.41
Wet snow albedo	0.6	0.5	1.24	1.28
		0.7	1.23	1.26
Melt lake albedo	0.05–0.40	−0.05	1.33	1.34
		+0.05	1.23	1.27
Initial surface density (kg m^{-3})	500	600	1.20	1.24
		400	1.22	1.27
Initial pore closure depth (m)	37	27	1.20	1.28
		47	1.26	1.30
Bottom boundary temperature gradient (K m^{-1})	0	+0.5	1.24	1.28
		−0.5	1.20	1.29
Initial surface temperature (K)	253	248	1.25	1.29
		258	1.29	1.30
Incoming shortwave radiation (W m^{-2})	0–841.89	×1.1	1.54	1.61
		×0.9	1.22	1.27

In order to account for this spin-up period, the calculations and comparisons below are carried out using the final 5 years of data from each simulation, unless specified otherwise. The results of the sensitivity tests for each parameter are discussed below.

6.1. Air Temperature

Both the average and maximum lake depth were found to vary with the air temperature. Increasing the air temperature by 0.5 K was found to increase the maximum lake depth by 0.1 to 1.34 m and the average lake depth was found to increase by 8.1%. As expected, in the opposite case, decreasing the average air temperature by 0.5 K was found to reduce the maximum lake depth over 5 years by 0.16 m and the average lake depth was reduced by 13.9%.

6.2. Lateral Melt Catchment Area

It would be expected that increasing the lateral melt water available would increase the average lake depth and vice versa. In order to test this, the model was run with both melt multiples of 3 and 9, the results of which are shown in Table 2.

As expected, meltwater from the catchment area plays a significant role in determining lake depth as well as in overall lake formation; there is an 85.2% increase in average lake depth between the 3X and 6X simulations, and further 35.8% increase from the 6X to the 9X value.

6.3. Accumulation

In order to determine the model's sensitivity to the addition of accumulation in the form of snow, tests were performed where the accumulation was halved and doubled compared to the reference case level of accumulation.

The level of accumulation can have three competing effects on the formation of lakes on an ice shelf. These all occur due to the density of fresh snow being less than that of compacted, older firn.

First of all, adding more accumulation will mean that there is a larger region of high pore fraction at the surface of the ice shelf. This means that a longer time is needed for the pore space to be saturated with meltwater and a lake created. Based on this, it would be expected that a greater level of accumulation would lead to shallower lakes, or no lakes at all. However, as the fresh snow is less dense than compacted, older firn, the second possibility is that more accumulation could lead to melting of a greater vertical distance into the firn for the same energy input. This can lead to quicker exposure of melt lakes and therefore to deeper lakes forming due to the change in albedo. Finally, less dense snow will have a lower thermal conductivity than denser firn meaning that surface temperature fluctuations do not propagate as far into the ice shelf. Heat will be gained or lost from a smaller surface layer, which will lead to a greater amplitude in surface temperature fluctuations. It is unclear what the result of this particular effect will be as this could both increase melting due to temperature increases at the surface, but also cause quicker refreezing as heat may be lost to the surroundings more quickly.

The interplay of these effects means that the response of the melt lakes to changes in accumulation can be complicated and is neither monotonic nor linear. In these cases examined here it seems that the second situation described above is occurring; an increase in the amount of snow leads to an increase in lake depth. The results of this are shown in Table 2. It appears that for this range of accumulation levels, the amount of snow available to melt is acting as a limiting factor for lake depth.

In addition to the above, the sensitivity of the model to the density of the accumulation was investigated. Once again, there will be competing effects of less dense snow meaning more pore space needs to be filled to saturate the firn, but less dense firn also requiring less energy to melt through the total snowfall.

It appears that here, in a similar way to adding greater amounts of less dense snow to the denser firn, decreasing the density of the snow also leads to deeper lakes. As shown in Table 2, both the average and maximum lake depths were increased through a reduction of the snow density to 300 kg m^{-3} (from the reference case value of 350 kg m^{-3}) and decreased through an increase of the snow density to 400 kg m^{-3}.

6.4. Dry Snow Densification

Section 2.1 describes the dry snow densification that is simulated by the model. In order to test the sensitivity of the model to this process, the model was run with the dry snow densification turned off. It was found that this meant that the initial ice lens formed 0.92 m further down in the firn and also that 5.1% more in situ melting was required for lens formation. Furthermore, the initial lake formed in the first year was less deep without dry snow densification than that of the reference case simulation. This would be expected given that without dry snow densification, there would be a greater amount of pore space to fill for saturation of the firn and a greater amount of refreezing of meltwater needed within any given level of the model for ice lens formation.

However, once the initial lake had formed and the amount of saturation of the firn needed for subsequent lake formation is much decreased (due to the previous year's refrozen lake acting as an impermeable layer meaning that only new snowfall needs to be melted or saturated), the lakes in the simulation with no dry snow densification become deeper than equivalent lakes in reference case simulation, with the average lake depth being 2.4% deeper in the case with no dry snow densification.

6.5. Foehn Winds

The foehn wind effect added to the model alters both the air temperature and the wind speed during the designated foehn wind events. Therefore, sensitivity tests were carried out on both of these values independently.

The modeled foehn wind events add 5 K to the observed AWS air temperature during their period of occurrence. Therefore, the change in temperature was examined by changing this value to both 3 and 7 K.

As would be expected, an increase in foehn wind temperature led to an increase in the average lake depth and vice versa, with an increase of 10.9% for a 2 K increase of temperature and a decrease of 3.5% for a 2 K decrease in temperature.

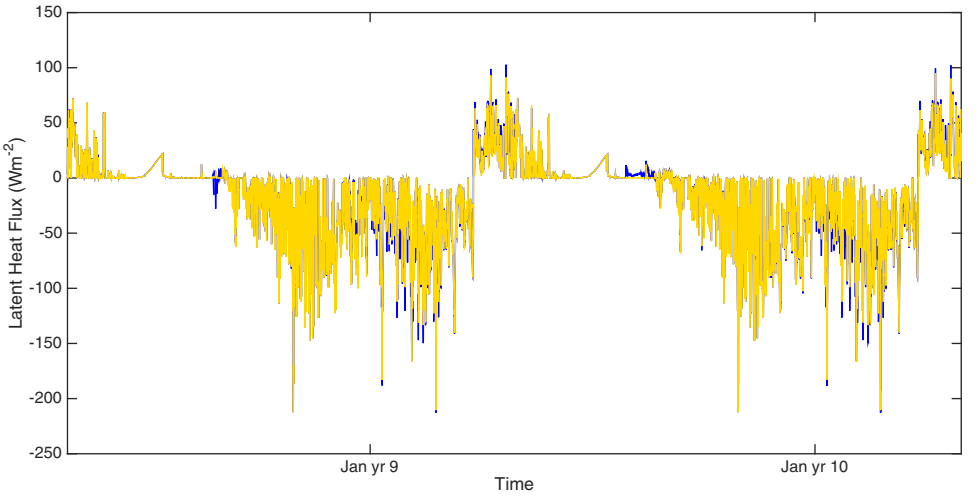

Figure 10. A comparison of the latent heat flux for the reference case (shown in yellow) plotted on top of the case where the foehn wind speed is increased by an extra 5 m s^{-1} up to 10 m s^{-1} (shown in blue).

The situation with the foehn wind speed is less straight forward as the wind speed affects both the sensible and latent heat. For the sensible heat, the sign of this effect is dependent on the air and surface temperature so, for example, an increase in wind speed could either increase or decrease the sensible heat. Likewise with the latent heat, the sign of the change can be positive or negative.

This leads to a nonmonotonic relationship between average lake size and wind speed. It was found that reducing the foehn wind speed below the reference case level by 5 m s^{-1} (to 0 m s^{-1}) causes a decrease of 4.3 cm in the average lake depth size, but increasing the wind speed by 5 m s^{-1} (to 10 m s^{-1}) causes a decrease in lake depth too, this time of 4.4 cm.

In order to determine the cause of this response of average lake depth to changes in wind speed, we can examine the sensible and latent heat fluxes separately. As can be seen in Figure 10, an increase in the foehn wind speed amplifies the latent heat for both positive and negative values. The increased positive values are around the time of lake formation so it could be expected that increased wind speed would increase lake depth based on the latent heat.

However, when we examine the sensible heat flux as shown in Figure 11 we can see that in comparison to the reference case, the addition of an extra 5 m s^{-1} of foehn wind speed on top of the reference case value

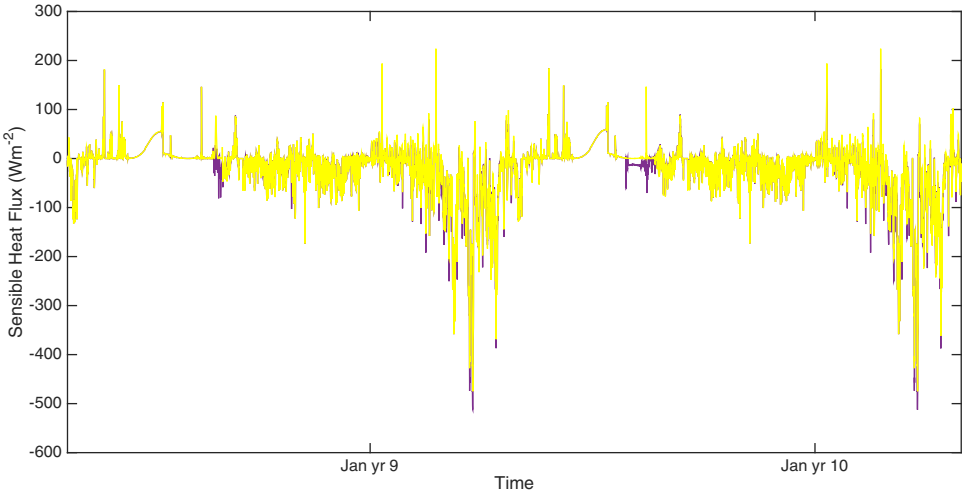

Figure 11. A comparison of the sensible heat flux for the reference case (shown in yellow) plotted on top of the case where the foehn wind speed is increased by an extra 5 m s^{-1} up to 10 m s^{-1} (shown in purple).

causes an increase in the magnitude mostly of the negative sensible heat values and this will be negating the positive influence of the latent heat flux that the wind is having during the time of lake formation somewhat, which would account for the reduced lake depths overall.

6.6. Wet Snow Albedo

The value of the wet snow albedo in the model is set as a constant which is used for the surface albedo once melting has begun, until the point that a lake is formed or the wet snow has refrozen. The sensitivity of the model to this parameter is tested by both reducing and increasing the chosen value for the wet snow albedo by 0.1 from the reference case value of 0.6 to 0.5 and 0.7, respectively.

Increasing the value of the albedo should mean that more shortwave radiation is reflected by the surface and therefore less energy is available for melting and smaller lakes would be expected. In contrast, it would be expected that reducing the value of the wet snow albedo would mean that less shortwave radiation is reflected and therefore more energy is absorbed and available for melting and deeper lakes would occur.

The sensitivity studies suggest that this is indeed the case, although the effect of the change in wet snow albedo did not lead to a large change in the lake depths. For an increase in the wet snow albedo value, the average lake depth is reduced by 1 cm, a reduction of less than 1% from the reference case simulation, and for the decrease in wet snow albedo, the average lake depth is increased by 0.1 cm, an increase of 0.1%. It was found that the overall melt was increased by reducing the wet snow albedo, especially during the spin-up period, but in the final 5 years of the simulation the difference was very little.

6.7. Melt Lake Albedo

The melt lake albedo is calculated from the formula given in equation (13) which is dependent on the lake depth. Here the albedo is varied by adding or subtracting 0.05 from the value calculated from this formula. This is a smaller variation than that made for the study of the wet snow albedo due to the fact that for deep lakes this could lead to the albedo becoming negative.

As expected, increasing the lake albedo leads to a reduction in both the average and maximum lake depths and reducing the lake albedo has the opposite effect.

6.8. Initial Density Profile

For the initial density profile input into the model, the empirical equation used (equation (19)) requires two choices of value: that for the surface density and that of the firn-ice transition, or pore closure depth. Therefore, both of these choices are examined here.

Despite an initial large effect on lake depth, with time the effect of changing the pore closure depth is much reduced. For the final 5 years of the simulations, there is a maximum of 3.1% difference between these simulations and the reference case for the average lake depth and a maximum of 1.4% difference for the maximum lake depth.

Second, the initial surface density is varied by increasing and decreasing the reference case value by 100 kg m^{-3}. The results from these two variations were as would be expected from the results of varying the pore closure depth; the higher density case resulted in a deeper average lake depth than the reference case and the lower density case resulted in shallower lakes. The denser the initial profile, the less melt water would be required to saturate the firn and therefore deeper lakes are possible with a less dense initial profile with the same amount of meltwater present. Again, this effect is reduced with time, despite large initial differences in lake depth both simulations tend toward similar values after the spin-up period. Examining the final 5 years, we see that there is a maximum of 2.7% difference between these simulations and the reference case for the average lake depth and a maximum of 3.4% difference for the maximum lake depth.

6.9. Bottom Boundary Condition

The assumption that the temperature gradient is zero at the bottom of the firn is tested by setting the gradient equal to a nonzero constant instead. The zero gradient condition was implemented as it was found during initial testing that temperature changes did not penetrate very far into the ice shelf on time scales of a few years (excluding the changes due to meltwater refreezing) so it is expected that if there is a temperature gradient within the middle of the ice shelf it is very small.

Here the values chosen to test the sensitivity of the model to this bottom boundary condition were 0.5 and -0.5 K m^{-1}. These values were chosen as values that could be physically realistic; the temperature gradients below 20 m in the ice cores used to determine the initial conditions rarely exceed 1 K m^{-1} and the most negative temperature gradient used at any point in the ice shelf in the modeling study of Holland and Jenkins (1999) is -0.125 K m^{-1}.

It was found that setting the bottom boundary condition equal to a constant gradient had no significant effect on the average lake depth. For the bottom boundary condition set to 0.5 K m^{-1}, the maximum and average lake depths did not vary from the reference case values (up to four decimal places). For the bottom boundary condition set to -0.5 K m^{-1}, the average lake depth varied by 3.1% from the reference case value and the maximum lake depth varied by only 0.4% from the reference case.

If we look at the initial 5 years of the model run we can see that the influence of the bottom boundary condition is even less; for the average lake depth over those 5 years the -0.5 K m^{-1} case only varies by 0.32% from the reference case. This suggests that the influence of the bottom boundary condition, although weak, increases with time. This is likely to be due to the meltwater penetrating deep into the top of the ice shelf in early years as the temperature change from this will take a long time to reach the bottom boundary of the model domain as heat is being transferred by conduction below the pore closure depth. This does suggest that for more accurate results a larger model domain could be used, but as the difference was only a small percentage here the 35 m profile was maintained for model efficiency.

6.10. Initial Temperature Profile

The initial temperature profile input into the model was examined by increasing and decreasing the initial surface temperature by 5 K. As the initial profile is based on a linear equation, this will change the whole initial temperature profile. For the final 5 years of the simulation, there was less than a 4.5% difference between average lake depth and the reference case for either simulation and a maximum difference of 1.2% for the maximum lake depth.

Although the initial lake depth is strongly influenced by the initial temperature profile, this quickly levels off and in later years the difference between the lake depths in these two cases is much reduced as the model loses memory of the initial temperature profile. However, there are still small differences between the reference case and these two simulations throughout the 10 years of the simulations. This suggests that although most of the effect of the initial temperature profile will be lost as long as an adequate spin-up period is applied, the lower grid cells of the model may still retain memory of the initial conditions as changes to them occur much more slowly.

6.11. Incoming Shortwave Radiation

The lake depth is expected to increase with increasing incoming shortwave radiation and this was found to be the case; multiplying the incoming shortwave radiation by a factor of 1.1 gave a 24.1% increase in the average lake depth (to a depth of 1.54 m) and a 25.6% increase in the maximum lake depth (to a depth of 1.61 m) when compared with the reference case simulation.

Similarly, a decrease in the incoming shortwave radiation showed a corresponding decrease in the average and maximum lake depths, but by a smaller percentage. When multiplying the incoming shortwave radiation by 0.9 we see a 1.6% decrease in the average lake depth and a 1.5% decrease in the maximum lake depth.

6.12. Comparison of Sensitivity

In order to directly compare the sensitivity of the model to some of the parameters tested above, we use a measure of model sensitivity as defined in Taylor and Feltham (2004). Here a nondimensional value, $d(x)$, is assigned as a measure of model sensitivity and is calculated as follows:

$$d(x) = \frac{\langle x \rangle}{\langle B \rangle} \frac{\partial(B)}{\partial(x)}. \tag{20}$$

Here $\langle x \rangle$ is a typical range of the parameter being examined, $\langle B \rangle$ is the typical value for the output of which the sensitivity is being tested, $\partial(B)$ is the range in that output value for the sensitivity studies, and $\partial(x)$ is the range of the parameter during the sensitivity studies.

Table 3
Values of the Sensitivity Parameter Given to Three Decimal Places

Parameter	Max lake depth sensitivity	Mean lake depth sensitivity
Accumulation amount	0.016	0.149
Accumulation density	−0.117	−0.106
Air temperature	0.214	0.205
Melt multiple	0.770	0.818
Wet snow albedo	−0.012	−0.010
Foehn wind temperature	0.089	0.100
Foehn wind speed	−0.031	0.001
Lake albedo	0.041	0.060
Shortwave radiation	0.233	0.246
Initial surface density	−0.019	−0.011
Initial firn-ice transition depth	0.020	0.047
Initial surface temperature	0.009	0.033
Bottom boundary condition	−0.004	0.031

For this study, two values for B are examined for each parameter, the maximum lake depth and the mean lake depth.

The typical range of a parameter is taken from the reference case simulation (e.g., the minimum to maximum air temperature from the reference case is used in the calculation for the air temperature simulation). Where a range of values is not available for the reference case (e.g., for the melt multiple which is set equal to a constant) then the total range of values used during the sensitivity studies is used here.

Table 3 shows the calculated values of this parameter for the sensitivity studies presented above for both the mean and maximum lake depths.

Given the size of the catchment area of the lakes, it is not surprising that the melt multiple value seems to be by far the most important parameter, demonstrating that topography is not only important in determining where lakes form, but is a key factor in determining the depth of the lakes that form too and suggesting that this is therefore a key area to focus future model developments.

From the values of the sensitivity parameter, it is clear that air temperature and shortwave radiation are also key parameters in determining lake depth, as is the snowfall and its density.

These results suggest that although foehn winds are key in lake formation, it seems from this study that the lake depths are more sensitive to the foehn wind temperature than the foehn wind speed. However, the lakes are less sensitive to foehn wind temperature than the overall air temperature suggesting that although foehn events are important in lake formation, an increase in air temperature would have a greater influence in lake depth. This is especially important given that an increase is predicted in climate models under future possible emissions scenarios (IPCC, 2013).

The initial conditions do not seem to have a large influence on the lakes beyond the first year, suggesting that once a lake has formed it alters the temperature and density profile of the ice shelf enough that conditions before this become insignificant in comparison to several other parameters, and that the spin-up period used here is adequate.

These initial conditions may become more important in a 3-D model, where 3-D fields for the firn density and temperature profiles, and free surface (topography) would be needed and the applied forcing will be a function of position as well as time. The initial density profile, for example, may be a relic of past meltwater percolation and refreeze events. The spatially varying forcing and topography may correspond to foehn winds in only part of the domain with explicit topographic steering of meltwater. The topography may correspond to the downstream expression of hummocks or crevices inherited from the ice sheet or grounding line. A 3-D model would allow examination of the "stability" problem, where the model is initiated with uniform topography and forcing and see if instability occurs (primarily via the albedo feedback but also through meltwater percolation and densification processes) and drives the formation of a melt lake.

Further details of these studies are available in Buzzard (2017a).

7. Conclusions

The appearance of melt lakes on an ice shelf can significantly alter the surface energy balance (primarily by lowering the albedo of the shelf), increase melt water production (and subsequent refreezing), and significantly alter the shelf's temperature and density profiles (see Figures 3 and 4). Melt lakes may also affect the mechanical stability of an ice shelf through hydrofracture and crevasse propagation.

We have developed a model of melt lakes on an ice shelf. Our model simulates the full life cycle of melt lakes (formation, evolution, and refreezing) and has been designed to be run over many years so that the impact of melt lakes on density and temperature profiles can be explored (previous models have been run for only one melt season).

The model calculates the transfer of heat through the upper ice shelf and incorporates the percolation and refreezing of meltwater through the firn. The effects of foehn winds and transport of water into a lake basin from a catchment area are considered. The model is the first of its kind to explicitly model the formation of ice lenses. It was found that the formation of solid ice lenses within the firn due to the refreezing of meltwater led to new model behaviour by enabling the formation of melt lakes, and that these lakes, once refrozen, in turn act as ice lenses in subsequent years leading to the more rapid formation of lakes.

While our model can theoretically be applied to any ice shelf (accepting the limitations covered in section 3.4), we have chosen to simulate conditions on the Larsen C Ice Shelf, as lakes have been observed there and it has been speculated that this ice shelf is vulnerable to melt lake-driven collapse under future warming conditions. Our simulations suggest that under current conditions surface melt lakes only form on the Larsen C Ice Shelf in locations where foehn winds are present. Topographic steering of meltwater was found to be key to the formation of melt lakes, which were found not to form without accounting for lateral transport of meltwater from its catchment area. Simulations carried out by altering the value of the melt multiple found that if a lake does not form there is 69.7% less surface melt than occurs in a lake basin when a lake does form, highlighting the importance of these features.

Our model predicts the formation of ice lenses on the Larsen C Ice Shelf and this was found to be consistent with in situ observations. Furthermore, the depth of lakes simulated by the model agree well with the deeper lake depths calculated from Landsat data.

Sensitivity studies show that the value chosen for the effective catchment area plays a key role in determining lake depth. We recommend that future model development focus on accounting for topographic steering of meltwater, perhaps through use of a detailed Digital Elevation Model. Air temperature and shortwave radiation are also important parameters in influencing lake depth.

Our model has shown the importance of melt lakes to ice shelf properties and that simulation of melt lakes depends on the representation of critical processes such as ice lens formation. While we have focused on the Larsen C Ice Shelf, the model can be used for any ice shelf with sufficient input data. Although the approach of using a fixed frame of reference for the catchment area does limit the applications the model could be adapted, for example for Greenland, if it was combined with a surface routing model. Furthermore, consideration would need to be made for the flow speed of any alternative locations modeled especially if they also experience localised conditions such as foehn winds. The model code has been made available at https://doi.org/10.17864/1947.121.

Acknowledgments
The authors acknowledge Allen Pope (NSIDC) for his contribution to the model validation, including the production of Figure 9 and calculation of lake depths from Landsat data. We also thank Amber Leeson and one anonymous reviewer for their helpful and thorough suggestions in improving this paper. S. Buzzard was supported by NERC Doctoral Training grant NE/J500082/1. The model code is publicly available in the following data repository: Buzzard (2017b).

References

Alexiades, V., & Solomon, A. (1993). *Mathematical modelling of melting and freezing processes*. Carlsbad, CA: Hemisphere Publishing Corporation.

Ambaum, M. H. P. (2010). Thermal physics of the atmosphere. *Advancing weather and climate science*. Chichester, UK: Wiley-Blackwell.

Arthern, R., Vaughan, D. G., Rankin, A., Mulvaney, R., & Thomas, E. (2010). In situ measurements of Antarctic snow compaction compared with predictions of models. *Journal of Geophysical Research: Earth Surface*, *115*, F03011. https://doi.org/10.1029/2009JF001306

Banwell, A., Arnold, N., Willis, I., Tedesco, M., & Ahlstrøm, A. (2012). Modeling supraglacial water routing and lake filling on the Greenland Ice Sheet. *Journal of Geophysical Research: Earth Surface*, *117*, F04012. https://doi.org/10.1029/2012JF002393

Banwell, A., MacAyeal, D., & Sergienko, O. (2013). Breakup of the Larsen B Ice Shelf triggered by chain reaction drainage of supraglacial lakes. *Geophysical Research Letters*, *40*, 5872–5876. https://doi.org/10.1002/2013GL057694

Bell, R. E., Studinger, M., Shuman, C. A., Fahnestock, M. A., & Joughin, I. (2007). Large subglacial lakes in East Antarctica at the onset of fast-flowing ice streams. *Nature*, *445*, 904.

Buzzard, S. (2017a). *Modelling melt lake formation on an ice shelf* (PhD thesis). Reading, UK: University of Reading.

Buzzard, S. (2017b). *A mathematical model of melt lake formation on an ice shelf*. Software. Reading, UK: University of Reading. https://doi.org/10.17864/1947.121

Clason, C., Mair, D., Burgess, D., & Nienow, P. (2012). Modelling the delivery of supraglacial meltwater to the ice/bed interface: Application to southwest Devon Ice Cap, Nunavut, Canada. *Journal of Glaciology*, *58*(208), 361–374.

Crank, J. (1984). *Free and moving boundary problems*. Gloucestershire, UK: Clarenden Press.

De Angelis, H., & Skvarca, P. (2003). Glacier surge after ice shelf collapse. *Science (New York, N.Y.)*, *299*(5612), 1560–1562.

Dimmler, W., Gutt, J., Barratt, I., Domack, E., Heilmayer, O., Isla, E., et al. (2011). Biodiversity change after climate-induced ice-shelf collapse in the Antarctic. *Deep Sea Research Part II: Topical Studies in Oceanography*, *58*, 74–83. https://doi.org/10.1016/j.dsr2.2010.05.024

Ebert, E., & Curry, J. (1993). An intermediate one-dimensional thermodynamic sea ice model for investigating ice-atmosphere interactions. *Journal of Geophysical Research: Oceans*, *98*(C6), 10085–10109.

Gladstone, R. M., Bigg, G. R., & Nicholls, K. W. (2001). Iceberg trajectory modeling and meltwater injection in the Southern Ocean, *106*(C9), 19903–19915.

Gourmelen, N., Shepherd, A., Jenkins, A., & Houlie, N. (2009). *Basal melt rate at the Larsen C Ice Shelf*. Poster c21d-0473 presented at the AGU Fall Meeting 2009, San Francisco, CA.

Henneman, H., & Stefan, H. (1999). Albedo models for snow and ice on a freshwater lake. *Cold Regions Science and Technology*, *29*, 31–48.
Holland, D. M., & Jenkins, A. (1999). Modeling thermodynamic ice-ocean interactions at the base of an ice shelf. *Journal of Physical Oceanography*, *29*(8), 1787–1800.
Hubbard, B., Luckman, A., Ashmore, D., Bevan, S., Kulessa, B., Kuipers Munneke, P., et al. (2016). Massive subsurface ice formed by refreezing of ice-shelf melt ponds. *Nature Communications*, *7*, 1–6. https://doi.org/10.1038/ncomms11897
IPCC. (2013). Annex I: Atlas of global and regional climate projections. In T. F. Stocker et al. (Eds.), *Climate change 2013: The physical science basis. Contribution of Working Group I to the fifth assessment report of the Intergovernmental Panel on Climate Change*. Cambridge, UK: Cambridge University Press.
Jarvis, E., & King, E. (1995). Seismic investigation of the Larsen Ice Shelf, Antarctica: In search of the Larsen Basin. *Antarctic Science*, *7*(2), 181–190.
Kingslake, J., Ely, J. C., Das, I., & Bell, R. E. (2017). Widespread movement of meltwater onto and across Antarctic ice shelves. *Nature*, *544*(7650), 349–352.
Kuipers Munneke, P., Van den Broeke, M., King, J., Grat, T., & Reijmer, C. (2012a). Near-surface climate and surface energy budget of Larsen C ice shelf, Antarctic Peninsula. *The Cryosphere*, *6*, 353–363.
Langley, E. S., Leeson, A. A., Stokes, C. R., & Jamieson, S. S. R. (2016). Seasonal evolution of supraglacial lakes on an East Antarctic outlet glacier. *Geophysical Research Letters*, *43*, 8563–8571. https://doi.org/10.1002/2016GL069511
Leeson, A., Shepherd, A., Palmer, S., Sundal, A., & Fettweis, X. (2012). Simulating the growth of supraglacial lakes at the western margin of the Greenland ice sheet. *The Cryosphere*, *6*(5), 1077–1086.
Leeson, A. A., Shepherd, A., Briggs, K., Howat, I., Fettweis, X., Morlighem, M., et al. (2015). Supraglacial lakes on the Greenland ice sheet advance inland under warming climate. *Nature Climate Change*, *5*, 51–55. https://doi.org/10.1038/nclimate2463
Ligtenberg, S., Helsen, M., & van den Broeke, M. (2011). An improved semi-empirical model for the densification of Antarctic firn. *The Cryosphere*, *5*, 809–819.
Luckmann, A., Elvidge, A., Jansen, D., Kulessa, B., Kuipers Munneke, P., King, J., et al. (2015). Surface melt and ponding on Larsen C Ice Shelf and the impact of foehn winds. *Antarctic Science*, *26*(6), 625–635.
Lüthje, M., Pedersen, L., Reeh, N., & Greuell, W. (2006). Modelling the evolution of supraglacial lakes on the West Greenland ice-sheet margin. *Journal of Glaciology*, *52*(179), 608–618.
MathWorks. (2015). *pdepe*. Retrieved from http://uk.mathworks.com/help/matlab/ref/pdepe.html
McKay, C., Clow, G., Anderson, D., & Wharton, R., Jr. (1994). Light transmission and reflection in perennially ice-covered Lake Hoare, Antarctica. *Journal of Geophysical Research: Oceans*, *99*(C10), 20427–20444.
Moaveni, S. (2010). *Engineering fundamentals: An introduction to engineering*. Boston, MA: Cengage Learning.
Morris, E., & Vaughan, D. (2003). Spatial and temporal variation of surface temperature on the Antarctic Peninsula and the limit of viability of ice shelves. In *Antarctic Peninsula climate variability: Historical and paleoenvironmental perspectives, Antarctic Research Series* (Vol. *79*). Washington, DC: American Geophysical Union.
Paterson, W. (2000). *The physics of glaciers*. Oxford, UK: Butterworth-Heinemann.
Pope, A., Scambos, T., Moussavi, M., Tedesco, M., Willis, M., Shean, D., et al. (2016). Estimating supraglacial lake depth in West Greenland using Landsat 8 and comparison with other multispectral methods. *The Cryosphere*, *10*(1), 15–27.
Rignot, E., Casassa, G., Gogineni, P., Krabill, W., Rivera, A., & Thomas, R. (2004). Accelerated ice discharge from the Antarctic Peninsula following the collapse of Larsen B ice shelf. *Geophysical Research Letters*, *31*, L18401. https://doi.org/10.1029/2004GL020697
Scambos, T., Bohlander, J., Schuman, C., & Skvarca, P. (2004). Glacier acceleration and thinning after ice shelf collapse in the Larsen B embayment, Antarctica. *Geophysical Research Letters*, *731*, L18402. https://doi.org/10.1029/2004GL020670
Scambos, T., Hulbe, C., & Fahnestock, M. (2003). Climate-induced ice shelf disintegration in the Antarctic Peninsula. In *Antarctic Peninsula climate variability, Antarctic Research Series* (Vol. 79). Washington, DC: American Geophysical Union.
Scambos, T., Hulbe, C., Fahnestock, M., & Bohlander, J. (2000). The link between climate warming and break-up of ice shelves in the Antarctic Peninsula. *Journal of Glaciology*, *46*(154), 516–530.
Schytt, V. (1958). *Glaciology. A: Snow studies at Maudheim. Glaciology. B: Snow studies inland. Glaciology. C: The inner structure of the ice shelf at Maudheim as shown by core drilling* (Norwegian-British-Swedish Antarctic Expedition, 1949-5, IV). Oslo, Norway: Norwegian Polar Institute.
Sergienko, O. (2005). *Surface melt in ice shelves and icebergs* (PhD thesis). Chicago, IL: University of Chicago.
Sergienko, O., & MacAyeal, D. (2005). Surface melting on Larsen Ice Shelf, Antarctica. *Annals of Glaciology*, *40*(1), 215–218.
Silva, T. A. M., Bigg, G. R., & Nicholls, K. W. (2006). Contribution of giant icebergs to the Southern Ocean freshwater flux. *Journal of Geophysical Research: Oceans*, *111*, C03004. https://doi.org/10.1029/2004JC002843
Singh, P. (2001). *Snow and glacier hydrology* (Vol. *37* of Water Science and Technology Library). Berlin, Germany: Springer Science & Business Media.
Skeel, R., & Berzins, M. (1990). A method for the spatial discretization of parabolic equations in one space variable. *SIAM Journal on Scientific and Statistical Computing*, *11*(1), 1–32.
Taylor, P., & Feltham, D. (2004). A model of melt pond evolution on sea ice. *Journal of Geophysical Research: Oceans*, *109*, C12007. https://doi.org/10.1029/2004JC002361
Tedesco, M., Lüthje, M., Steffen, K., Steiner, N., Fettweis, X., Willis, I., et al. (2012). Measurement and modeling of ablation of the bottom of supraglacial lakes in western Greenland. *Geophysical Research Letters*, *39*, L02502. https://doi.org/10.1029/2011GL049882
Tseng, P., Illangasekare, T., & Meier, M. (1994). Modelling of snow melting and uniform wetting front migration in a layered subfreezing snowpack. *Water Resources Research*, *30*(8), 2363–2376.